

arXiv:2504.09366v2 [quant-ph] 11 Jul 2025

Chapter 4

Quantum Rabi oscillations in the semiclassical limit: backreaction on the cavity field and entanglement

Alexandre P. Costa¹ and Alexandre Dodonov^{1,2,a}

¹ Institute of Physics, University of Brasilia, 70910-900, Brasilia, DF, Brazil

² International Center of Physics, Institute of Physics, University of Brasilia, 70910-900, Brasilia, DF, Brazil

^aadodonov@unb.br

4.1 Abstract

The goal of this chapter is to compare the predictions of the semiclassical Rabi model (SRM), which describes the interaction between a two-level system (qubit) and a classical monochromatic wave, and the quantum Rabi model (QRM), under the assumption that the cavity field is initiated in a coherent state with a large average number of photons, ranging from 5.000 to 40.000. First, we show that for a strong atom–field coupling, when the duration of the π -pulse (the time interval required to completely excite or deexcite the qubit in the resonant regime) is below $100\omega^{-1}$, the behaviour of the atomic excitation probability deviates significantly from the textbook sinusoidal formula derived for the SRM under the rotating-wave approximation, and we present simple analytical and semi-analytical methods to describe more accurately the dynamics. Then we show that the QRM reproduces the qubit’s dynamics predicted by the SRM only for initial times, since in the QRM the qubit excitation probability exhibits a collapse behaviour even in the lossless scenario; we also notice that the qualitative behaviour of such collapses is different from the ones occurring in the dissipative SRM. In the rest of this work we study numerically the backreaction of the qubit on the cavity field and the resulting

atom–field entanglement, which are disregarded in the SRM. It is shown that the atom–field entanglement increases over time and a maximally entangled state is attained for large times. Moreover, we illustrate how the Rabi oscillations continuously modify the quantum state of the cavity field, which becomes increasingly different from the original coherent state as the time increases.

4.2 Introduction

Rabi oscillations or Rabi flopping of a two-level system (that we also call qubit, or atom, for short) constitute an invaluable tool in the area of Quantum Information and Quantum Computing, as they allow for the implementation of single-qubit quantum gates, readout of the qubit’s state, measurement of the coherence properties of qubits, etc [1–3]. The Rabi oscillations, first studied by I. I. Rabi in the context of a spin in a classical rotating magnetic field [4, 5], correspond to the periodic oscillation of the atomic population inversion due to a drive by a resonant or near-resonant classical field, and take place in a plethora of physical systems, such as nuclear magnetic resonance, cold atoms, impurity states in insulators, quantum dots, superconducting circuits, Rydberg atoms, cavity polaritons, etc. [6]. It is probably one of the first examples of the light–matter interaction one learns when studying Quantum Optics or Atomic Physics, since a simple analytical solution can be obtained after invoking the Rotating Wave Approximation (RWA) [7–9]. The mathematical description of the interaction between a quantum two-level system and a periodically time-varying classical field has become known as the semiclassical Rabi model (SRM), and many analytic approaches were developed to determine its spectral and dynamical properties beyond the RWA [10–14] or in the presence of external modulations [15–19].

When the driving field is treated quantum mechanically, the mathematical description is given by the quantum Rabi model (QRM) [20–23], and the transition from the quantum to the semiclassical regime as the field intensity increases has been recently investigated in [24, 25]. Since we know that the electromagnetic field is quantized, it is obvious that the SRM is an idealization of the actual interaction between the qubit and a coherent field state with large amplitude; hence the qubit must become entangled with the field during the evolution (at the very least, during some time intervals), and also modify the field state. Here we study, first, the degree of entanglement between the qubit and the cavity field in the semiclassical limit, in order to assess the intrinsic limitations for the purity of the qubit (due to the quantized nature of the electromagnetic field) during the operation of quantum gates based on the Rabi flopping. Second, we analyse the modifications of the cavity field state due to the Rabi oscillations, discussing whether the semiclassical assumption that the field remains forever in the initial coherent state is justifiable. Our findings, based on numeric simulations involving relatively large average photon numbers and long time intervals, can be used to estimate the situations in which the SRM is sufficiently accurate to describe the qubit behaviour.

4.3 Semiclassical Rabi model

Consider a two-level system with the ground and excited states $|g\rangle$ and $|e\rangle$, respectively, and the energy difference $\hbar\Omega$, where \hbar is the Planck constant and Ω is the atomic transition

frequency. The interaction of the atom with a classical monochromatic electromagnetic field of frequency ω is described by the celebrated semiclassical Rabi Hamiltonian [6–9]

$$\hat{H}/\hbar = \frac{\Omega}{2}\hat{\sigma}_z + G(\hat{\sigma}_+ + \hat{\sigma}_-) \cos(\omega t) , \quad (4.1)$$

where the semiclassical light–matter coupling parameter G is known as the Rabi frequency, and the atomic operators are $\hat{\sigma}_z = |e\rangle\langle e| - |g\rangle\langle g|$, $\hat{\sigma}_+ = |e\rangle\langle g|$ and $\hat{\sigma}_- = \hat{\sigma}_+^\dagger = |g\rangle\langle e|$. To derive the qubit dynamics one needs to solve the Schrödinger equation

$$i\frac{\partial|\psi\rangle}{\partial t} = \frac{\hat{H}}{\hbar}|\psi\rangle . \quad (4.2)$$

Making the unitary transformation, $|\psi(t)\rangle = e^{-i\omega t\hat{\sigma}_z/2}|\psi_1(t)\rangle$, the new wavefunction $|\psi_1\rangle$ obeys the Schrödinger equation with the Hamiltonian

$$\hat{H}^{(1)} = \hat{H}_r + \hat{H}_{cr} , \quad (4.3)$$

where

$$\hat{H}_r/\hbar = -\frac{\Delta}{2}\hat{\sigma}_z + \frac{G}{2}(\hat{\sigma}_+ + \hat{\sigma}_-) \quad (4.4)$$

$$\hat{H}_{cr}/\hbar = \delta\frac{G}{2}(e^{2it\omega}\hat{\sigma}_+ + e^{-2it\omega}\hat{\sigma}_-) . \quad (4.5)$$

\hat{H}_r is the time-independent “rotating” Hamiltonian, and \hat{H}_{cr} is the time-dependent “counter-rotating” Hamiltonian due to the counter-rotating terms. We also defined the detuning $\Delta = \omega - \Omega$ and the dichotomous parameter $\delta = \{0, 1\}$: for $\delta = 1$ we have the complete case, while $\delta = 0$ implies the RWA.

The eigenvalues of \hat{H}_r are easily found as $E_{\pm} = \pm\hbar R/2$, where $R = \sqrt{G^2 + \Delta^2}$. The corresponding eigenstates are

$$|\phi_{\pm}\rangle = \sqrt{\frac{1}{RR_{\pm}}}\left(R_{\pm}|g\rangle \pm \frac{G}{2}|e\rangle\right) , \quad (4.6)$$

where we defined $R_{\pm} = (R \pm \Delta)/2$. In particular, in the *resonant regime*, $\Delta = 0$, we have $R = G$, $R_{\pm} = G/2$ and $|\phi_{\pm}\rangle = (|g\rangle \pm |e\rangle)/\sqrt{2}$. From Eq. (4.6) one can easily calculate all the matrix elements $\langle\phi_l|\hat{\sigma}_i|\phi_k\rangle$, where $l, k = \pm$ and $\hat{\sigma}_i$ stand for any qubit operator.

The solution of the Schrödinger equation for the Hamiltonian $\hat{H}^{(1)}$ can be found by expanding the system state in terms of the eigenstates of \hat{H}_r as [26]

$$|\psi_1\rangle = e^{-iE_{-}t} [e^{-iRt}A_{+}(t)|\phi_{+}\rangle + A_{-}(t)|\phi_{-}\rangle] , \quad (4.7)$$

where $A_{\pm}(t)$ are the probability amplitudes, and for the initial state $|\psi(0)\rangle = c_g|g\rangle + c_e|e\rangle$ one has

$$A_{\pm}(0) = \sqrt{\frac{1}{RR_{\pm}}}\left(R_{\pm}c_g \pm \frac{G}{2}c_e\right) . \quad (4.8)$$

From Eq. (4.7), the atomic excitation probability reads

$$P_e = |\langle e|\psi(t)\rangle|^2 = \left(\frac{G}{2R}\right)^2 \left| \sqrt{\frac{R}{R_{+}}}A_{+}(t)e^{-iRt} - \sqrt{\frac{R}{R_{-}}}A_{-}(t) \right|^2 . \quad (4.9)$$

Analogously, all the other atomic properties can be determined from the knowledge of $|\psi_1\rangle$.

Under the RWA, $\delta = 0$, the probability amplitudes A_{\pm} become time-independent, and for the exact resonance, $\Delta = 0$, one obtains the textbook expression [7, 8]

$$P_e = \sin^2 \frac{Gt}{2} + |c_e|^2 \cos Gt - \text{Im} (c_e c_g^*) \sin Gt . \quad (4.10)$$

In particular, for the “ π -pulse”, corresponding to the time interval $T_{\pi} = \pi/G$, the complete transition $|g\rangle \leftrightarrow |e\rangle$ is accomplished.

Without the RWA, setting $\delta = 1$, one has to solve the differential equations

$$i\dot{A}_+ = \frac{G^2}{2R} \cos(2\omega t) A_+ + e^{itR} \frac{G}{2R} (R_- e^{2i\omega t} - R_+ e^{-2i\omega t}) A_- \quad (4.11)$$

$$i\dot{A}_- = -\frac{G^2}{2R} \cos(2\omega t) A_- + e^{-itR} \frac{G}{2R} (R_- e^{-2i\omega t} - R_+ e^{2i\omega t}) A_+ . \quad (4.12)$$

Defining new time-dependent probability amplitudes $a_{\pm}(t)$ via the transformation

$$A_{\pm}(t) = e^{\mp i\Upsilon \sin(2\omega t)/2} a_{\pm}(t) , \quad (4.13)$$

where we defined the dimensionless parameter

$$\Upsilon \equiv \frac{G^2}{2\omega R} , \quad (4.14)$$

we obtain the exact differential equations

$$\dot{a}_+ = -iQ_t a_- , \quad \dot{a}_- = -iQ_t^* a_+ \quad (4.15)$$

with

$$Q_t = \frac{G}{2R} e^{i[\Upsilon \sin(2\omega t) + Rt]} (R_- e^{2i\omega t} - R_+ e^{-2i\omega t}) . \quad (4.16)$$

In this work we focus on the resonant regime, $\Delta = 0$, for which $\Upsilon = G/2\omega$ and

$$Q_t = \frac{G}{4} e^{i\Upsilon \cos(2\omega t - \pi/2)} e^{iRt} (e^{2i\omega t} - e^{-2i\omega t}) . \quad (4.17)$$

For the solution of Eqs. (4.15) near the multi-photon resonances, $\Omega \approx (2n + 1)\omega$, see [17, 26]. In our present case of one-photon resonance, from the Jacobi-Anger expansion we write

$$e^{i\Upsilon \cos \theta} = J_0(\Upsilon) + \sum_{n=1}^{\infty} i^n J_n(\Upsilon) (e^{i\theta n} + e^{-i\theta n}) , \quad (4.18)$$

where

$$J_n(\Upsilon) = \sum_{k=0}^{\infty} \frac{(-1)^k}{k!(n+k)!} \left(\frac{\Upsilon}{2}\right)^{n+2k} \quad (4.19)$$

is the Bessel function of the first kind, with the known property $J_n(-x) = (-1)^n J_n(x)$. Assuming the realistic condition $\Upsilon \ll 1$ and keeping only the three initial terms in the expansion (4.18), we obtain

$$Q_t \approx i \frac{G}{2} [(J_0 - J_2) \sin 2\omega t + iJ_1] e^{iGt} , \quad (4.20)$$

where we used the short-hand notation $J_k \equiv J_k(\Upsilon)$. By solving numerically Eqs. (4.15) with Q_t given by Eq. (4.20) one finds the atomic excitation probability

$$P_e = \frac{1}{2} \left| e^{-i[\Upsilon \sin(2\omega t) + Gt]} a_+ - a_- \right|^2. \quad (4.21)$$

We call this an approximate *semi-analytic solution*, since a_{\pm} still has to be determined by solving somehow Eqs. (4.15) together with Q_t given by Eq. (4.20). A simple closed approximate analytic solution, better than the RWA solution, Eq. (4.10), can be obtained by neglecting the rapidly oscillating term proportional to $\sin 2\omega t$ in Eq. (4.20). The resulting differential equations

$$\dot{a}_{\pm} = i \frac{G}{2} J_1 e^{\pm i G t} a_{\mp} \quad (4.22)$$

can be easily cast as second-order differential equations

$$\ddot{a}_{\pm} \mp i G \dot{a}_{\pm} + \left(\frac{G J_1}{2} \right)^2 a_{\pm} = 0. \quad (4.23)$$

The solutions read

$$a_+(t) = e^{i G t / 2} \left[b_1 e^{i G s t / 2} + b_2 e^{-i G s t / 2} \right] \quad (4.24)$$

$$a_-(t) = \frac{e^{-i G t / 2}}{J_1} \left[b_1 (1 + s) e^{i G s t / 2} + b_2 (1 - s) e^{-i G s t / 2} \right], \quad (4.25)$$

where $s = \sqrt{1 + J_1^2}$. The coefficients b_1 and b_2 are determined from the initial condition (4.8) as

$$b_1 = \frac{(s - 1 + J_1) c_g + (s - 1 - J_1) c_e}{2\sqrt{2}s} \quad (4.26)$$

$$b_2 = \frac{(s + 1 - J_1) c_g + (s + 1 + J_1) c_e}{2\sqrt{2}s}. \quad (4.27)$$

For the lack of a better name, we call this solution an “*intermediate*” solution, since it partially takes into account the counter-rotating terms.

To test the validity of the approximate methods, we solved numerically Eqs. (4.15) – (4.16), which describe exactly the dynamics of the SRM, and compared the results to the predictions of the RWA, intermediate, and semi-analytical solutions. We considered the resonant regime, $\Delta = 0$, and the initial ground state, $|\psi(0)\rangle = |g\rangle$. Figure 4.1 shows the behaviour of the atomic excitation probability P_e as a function of time for three different coupling strengths, parametrized in terms of the duration of the π -pulse: $\omega T_{\pi} = 500$ (panel 4.1a, with the zoom in the panel 4.1d), $\omega T_{\pi} = 50$ (panel 4.1b, with zoom in panel 4.1e) and $\omega T_{\pi} = 15$ (panel 4.1c, with zoom in panel 4.1f); the corresponding Rabi frequencies read $G/\omega = \pi/(\omega T_{\pi})$. The red lines show the standard RWA solution, Eq. (4.10), while the black lines depict the semi-analytical solution, which for the considered parameters is indistinguishable from the exact numeric solution. The blue lines depict the intermediate solution, which is quite precise for relatively small coupling strengths, $\omega T_{\pi} \gtrsim 50$, and initial times, $\omega t \lesssim 10^3$, but loses accuracy as the time increases.

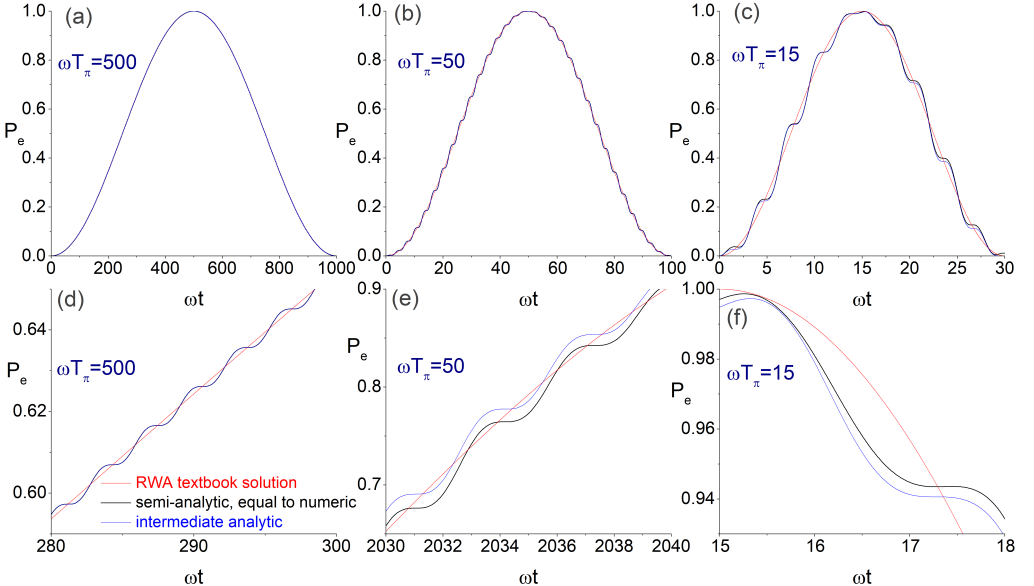


Figure 4.1: Atomic excitation probability as function of the dimensionless time for the lossless SRM. The Rabi frequencies, $G = \pi/T_\pi$, are parametrized in terms of T_π as: a) $T_\pi = 500\omega^{-1}$. b) $T_\pi = 50\omega^{-1}$. c) $T_\pi = 15\omega^{-1}$. Red lines depict the RWA solution. Black lines depict the semi-analytic solution, which is indistinguishable from the exact numeric solution for the chosen parameters. Blue lines depict the intermediate analytic solution. d-f) Zooms of the panels (a-c) illustrating the discrepancies between different solutions.

This can be clearly seen in the panels 4.1d – 4.1f, which show the discrepancies between different approximate methods. On the other hand, for very short pulses, $\omega T_\pi \lesssim 15$, the intermediate solution is inaccurate even for the initial times, $t \sim T_\pi$, while the semi-analytic solution holds perfectly. These results by no means imply that one cannot use the resonant light–matter interaction to control the qubit state. Instead, they show that to accurately control the atomic state one cannot rely on the standard RWA expression for “short” pulses with $\omega T_\pi \lesssim 500$, and a more accurate approach is necessary (e.g., the semi-analytic or the exact numeric solutions).

However, for an accurate preparation and control of the qubit state, as required in many protocols in the areas of Quantum Information and Quantum Computing, one also needs to know the degree of qubit’s purity. One obvious reason for non-unitary purity is the dissipative effects, which arise from the interaction of the qubit with its surroundings, so the qubit dynamics must be described by some master equation for the density operator $\hat{\rho}$. A fairly accurate approach consists in employing the “standard” Markovian master equation of Quantum Optics [27, 28]

$$\frac{\partial \hat{\rho}}{\partial t} = -i \left[\hat{H}/\hbar, \hat{\rho} \right] + \frac{\gamma}{2} (n_{th} + 1) \mathcal{D}[\hat{\sigma}_-] \hat{\rho} + \frac{\gamma}{2} n_{th} \mathcal{D}[\hat{\sigma}_+] \hat{\rho} + \frac{\gamma_\phi}{2} \mathcal{D}[\hat{\sigma}_z] \hat{\rho}, \quad (4.28)$$

where γ is the damping rate, γ_ϕ is the pure dephasing rate, $\mathcal{D}[\hat{\sigma}_k] \hat{\rho} \equiv 2\hat{\sigma}_k \hat{\rho} \hat{\sigma}_k^\dagger - \hat{\sigma}_k^\dagger \hat{\sigma}_k \hat{\rho} -$

$\hat{\rho}\hat{\sigma}_k^\dagger\hat{\sigma}_k$ is the Lindblad superoperator and $n_{th} = [e^{\hbar\Omega/k_B T} - 1]^{-1}$ is the average thermal photon number for the reservoir's temperature T (k_B is the Boltzmann constant). This equation will be used in the next section with $n_{th} = 0.05$ to calculate numerically the purity of the qubit, as well as the actual dynamics in the dissipative case (for an approximate solution of this master equation near multi-photon resonances see [18, 19, 26]). Another reason for non-unitary purity is the inevitable entanglement between the atom and the cavity field due to their interaction – a phenomenon overlooked in the semiclassical model, that requires the quantized description of the cavity field. So in the next section we shall study numerically the QRM to find out how the qubit and the field get entangled throughout the evolution and how this fact drastically affects the purity (and the overall behavior) of the system.

4.4 Quantum Rabi model

The quantum Rabi model [20–22] is described by the Hamiltonian

$$\hat{H}_{QRM}/\hbar = \frac{\Omega}{2}\hat{\sigma}_z + \omega\hat{n} + g(\hat{a} + \hat{a}^\dagger)(\hat{\sigma}_+ + \hat{\sigma}_-), \quad (4.29)$$

where ω is the resonant frequency of the cavity, \hat{a} and \hat{a}^\dagger are the annihilation and creation operators of the electromagnetic field, $\hat{n} = \hat{a}^\dagger\hat{a}$ is the photon number operator and g is the one-photon light-matter coupling constant. Although the QRM is exactly solvable [22], the analytic solution is cumbersome, and in many cases the counter-rotating terms $(\hat{a}\hat{\sigma}_- + \hat{a}^\dagger\hat{\sigma}_+)$ are neglected to obtain the easily solvable Jaynes-Cummings Hamiltonian [8, 29]. But here we solve numerically the complete Hamiltonian (4.29).

Let us briefly see how the quantum Rabi Hamiltonian is related to the semiclassical one, Eq. (4.1). The infinite-dimensional state space of the cavity electromagnetic field is spanned by the Fock states $|n\rangle$, where $n = 0, 1, 2, \dots$, so the state of the total atom-field system can be expanded as

$$|\Psi(t)\rangle = \sum_{n=0}^{\infty} [A_n(t)|g\rangle + B_n(t)|e\rangle] \otimes |n\rangle. \quad (4.30)$$

Defining a new wavefunction $|\Psi_1(t)\rangle$ as $|\Psi(t)\rangle = \exp(-i\omega\hat{n}t)|\Psi_1(t)\rangle$, we trivially find that $|\Psi_1(t)\rangle$ obeys the Schrödinger equation with the time-dependent Hamiltonian

$$\hat{H}_{QRM}^{(1)}/\hbar = \frac{\Omega}{2}\hat{\sigma}_z + g(\hat{a}e^{-i\omega t} + \hat{a}^\dagger e^{i\omega t})(\hat{\sigma}_+ + \hat{\sigma}_-). \quad (4.31)$$

Let us assume that the cavity is prepared initially in the coherent state (without loss of generality, we assume that α is real)

$$|\alpha\rangle = e^{-\alpha^2/2} \sum_{n=0}^{\infty} \frac{\alpha^n}{\sqrt{n!}} |n\rangle. \quad (4.32)$$

Recalling that $\hat{a}|\alpha\rangle = \alpha|\alpha\rangle$, let us postulate that *the cavity field remains permanently in this state*, no matter what. Then, the total system density operator is given by $\hat{\rho}_{tot} =$

$\hat{\rho} \otimes |\alpha\rangle\langle\alpha|$, where $\hat{\rho}$ is the qubit's density operator, and the qubit dynamics is governed by the Hamiltonian

$$\hat{H}_q/\hbar = \text{Tr}_f \left[\hat{H}_{QRM}^{(1)}/\hbar \otimes |\alpha\rangle\langle\alpha| \right] = \frac{\Omega}{2} \hat{\sigma}_z + g\alpha (e^{-i\omega t} + e^{i\omega t}) (\hat{\sigma}_+ + \hat{\sigma}_-) , \quad (4.33)$$

which reduces to the semiclassical Hamiltonian (4.1) with the identification $G = 2g\alpha$. In the above formula Tr_f denotes the partial trace over the field. For a rigorous analysis of the transition from QRM to SRM see Refs. [24, 25].

For the numeric simulations, we make use of the Gaussian profile of the photon number distribution of $|\alpha\rangle$ for large average photon numbers, $\langle\hat{n}\rangle = \langle\alpha|\hat{n}|\alpha\rangle = \alpha^2 \gg 1$. From the asymptotic expansion

$$|\langle n|\alpha\rangle|^2 \simeq \frac{1}{\sqrt{2\pi}\Delta n} \exp \left[- \left(\frac{n - (\langle\hat{n}\rangle - 1/2)}{\sqrt{2}\Delta n} \right)^2 \right] , \quad (4.34)$$

where $\Delta n = \sqrt{\langle n^2 \rangle - \langle n \rangle^2} = \alpha$ is the standard deviation, we see that the photon number probability is centered at $\langle\hat{n}\rangle - 1/2$ and goes to zero when $|n - \alpha^2| \gg \alpha$. In this work we consider the dynamical regime in which there is no creation nor annihilation of a significant number of excitations (a tiny number of such excitations is naturally generated due to the counter-rotating terms of the Rabi Hamiltonian, but they are negligible unless $g\alpha \sim \omega$ or there are resonant external modulations [30–32]), so we truncate the state (4.30) as

$$|\Psi(t)\rangle = \sum_{n=N_1}^{N_2} (A_n(t)|g\rangle + B_n(t)|e\rangle) \otimes |n\rangle , \quad (4.35)$$

where N_1 and N_2 are chosen so that for the initial state $|\Psi(0)\rangle = |g\rangle \otimes |\alpha\rangle$ one has $A_n(0) < 10^{-10}$ for $n \notin [N_1, N_2]$. For concreteness, the values we use are (K stands for 10^3):

Value of $\langle\hat{n}\rangle = \alpha^2$	N_1	N_2
5K	4,309	5,723
10K	9,019	11,013
20K	18,746	21,280
30K	28,299	31,733
40K	38,036	41,996

In the following section we solve the coupled ordinary differential equations for A_n and B_n , obtained from the Schrödinger equation with the Hamiltonian \hat{H}_{QRM} , via the Runge-Kutta-Verner fifth-order and sixth-order method. We consider the initial state $|g\rangle \otimes |\alpha\rangle$, exact atom–field resonance ($\Delta = 0$) and set the one-photon coupling constant through the condition $g\alpha/\omega = 10^{-2}\pi$, which corresponds to the constant π -pulse duration $\omega T_\pi = 50$ for any value of $\alpha \gg 1$.

4.4.1 Evolution of P_e in QRM

In Fig. 4.2 we show the dynamics of the atomic excitation probability for SRM and QRM, obtained by solving numerically the master equation (4.28) and the Schrödinger equation

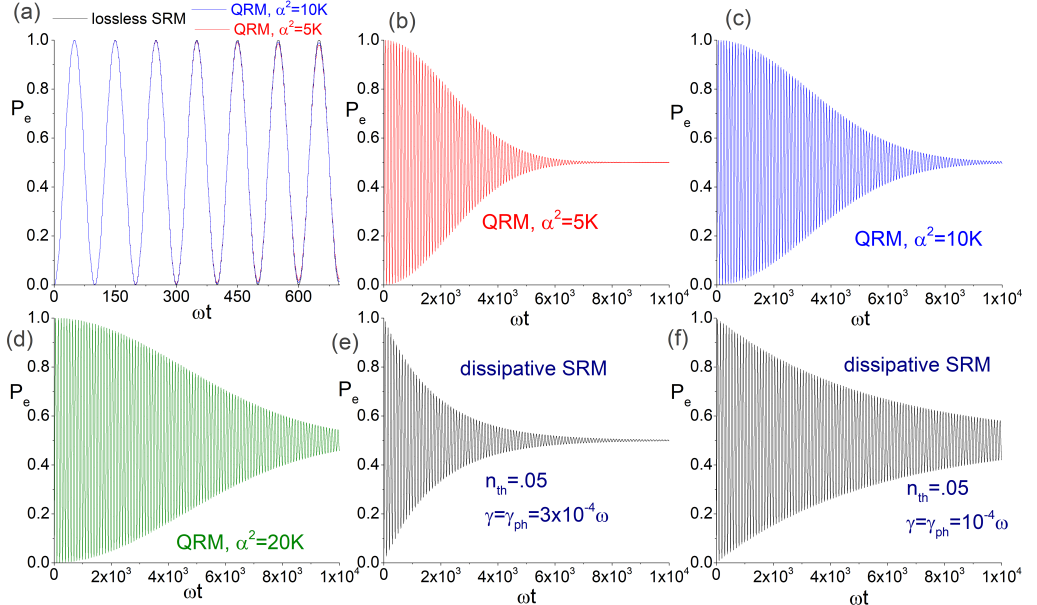


Figure 4.2: Atomic excitation probability as function of time in different scenarios. a) Comparison of the lossless SRM (black line, representing the exact numeric solution and the semi-analytic one, which are indistinguishable in this case) to the QRM for $\alpha^2 = 5K$ and $10K$. b-d) QRM for $\alpha^2 = 5K$, $10K$ and $20K$. e-f) Numeric solution of the SRM in the presence of dissipation for the dissipative parameters indicated in the plots. Notice that the behavior of P_e is quantitatively different in the dissipative SRM and the lossless QRM, although in both cases P_e undergoes a collapse.

with the Hamiltonian (4.29), respectively. Panel 4.2a shows the dynamics for initial times without dissipation. We see that for $t \lesssim 5T_\pi$ the semiclassical results are almost indistinguishable from the quantum ones, even for a relatively weak coherent state with $\alpha^2 = 5K$ (and the agreement becomes better as α increases). Therefore, for a few Rabi oscillations and ‘‘classical’’ fields (with $\alpha^2 \gtrsim 5K$, for our parameters) the semi-analytic formula can be used (with a negligible error) the behaviour of P_e .

However, for larger times the predictions of quantum and semiclassical models start to differ qualitatively due to the characteristic collapse behaviour, present in the quantum case at the typical timescales $\omega T_{\text{col}} \sim \pi\omega/2g = \alpha\omega T_\pi$, which for our parameters means $\omega T_{\text{col}} \sim 50\alpha$. This estimate can be obtained following the standard arguments of destructive interference of the quantum Rabi oscillations corresponding to different photon numbers [8, 33], and is attested by the Figures 4.2 and 4.3. By the same arguments, the revival time is estimated as

$$(\omega T_{\text{rev}}) \sim \frac{2\pi\alpha\omega}{g} = 4\alpha^2(\omega T_\pi) = 200\alpha^2, \quad (4.36)$$

so even for $\alpha^2 = 5K$ it would occur at $\omega T_{\text{rev}} \sim 10^6$. For such long time intervals the dissipation would alter completely the dynamics, so it seems unrealistic to study theoretically

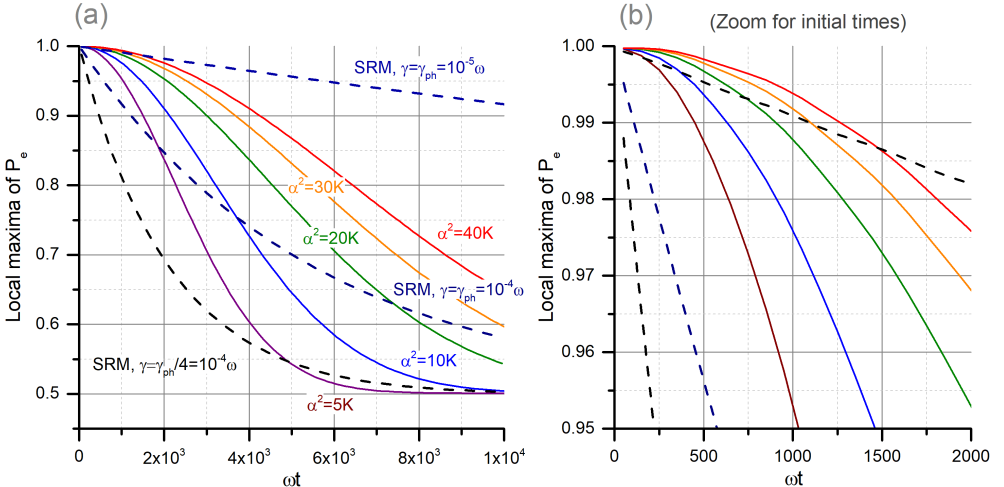


Figure 4.3: Behaviour of the local maxima of P_e as function of time for dissipative SRM (dashed lines, with $n_{th} = 0.05$) and lossless QRM (solid lines). The dissipative parameters and the values of α^2 are indicated in the figure. The panel (b) is the zoom of (a) for initial times. Notice that in the QRM the collapse time T_{col} scales as α .

the revivals for such coherent states without taking the dissipation into account, hence we do not pursue this subject here.

Notice also that the collapse behaviour of P_e in the quantum model is qualitatively different from the semiclassical collapse due to dissipation. This is illustrated in panels 4.2e and 4.2f, where we solved numerically the master equation for the parameters indicated in the figure. Although the atomic population also goes asymptotically to 1/2, the behaviour of the envelope (denoting the local maxima of P_e during the Rabi oscillations) is clearly different. This is most clearly seen in Figure 4.3, where we illustrate the behaviour of the local maxima of P_e . This figure confirms that the collapse time indeed scales approximately as $\omega T_{col} \sim 50\alpha$ (for instance, notice that the time for which $P_e = 0.6$ for $\alpha^2 = 20K$ is precisely twice the corresponding time for $\alpha^2 = 5K$), and the decay of the envelope is strikingly different in the QRM and dissipative SRM.

4.4.2 Backreaction on the cavity field and entanglement

Finally, we proceed to study some important features overlooked in the semiclassical model: the backreaction of the atom on the cavity field (which modifies the field state) and the atom-field entanglement (which lowers the qubit purity). We notice that the backreaction of the atom on the field has been studied in the past [14], however, we believe that the numerical analysis presented here complements nicely the previous results.

In Fig. 4.4 we show the variation of the cavity average photon number, $\Delta n = \langle \hat{n}(t) \rangle - \langle \hat{n}(0) \rangle$ as a function of time. In the panels 4.4a – 4.4d we consider a single-qubit QRM with $\alpha^2 = 5K, 10K, 20K$ and $30K$, respectively. As expected intuitively, the cavity field exchanges one photon with the qubit, and the average photon number also undergoes a

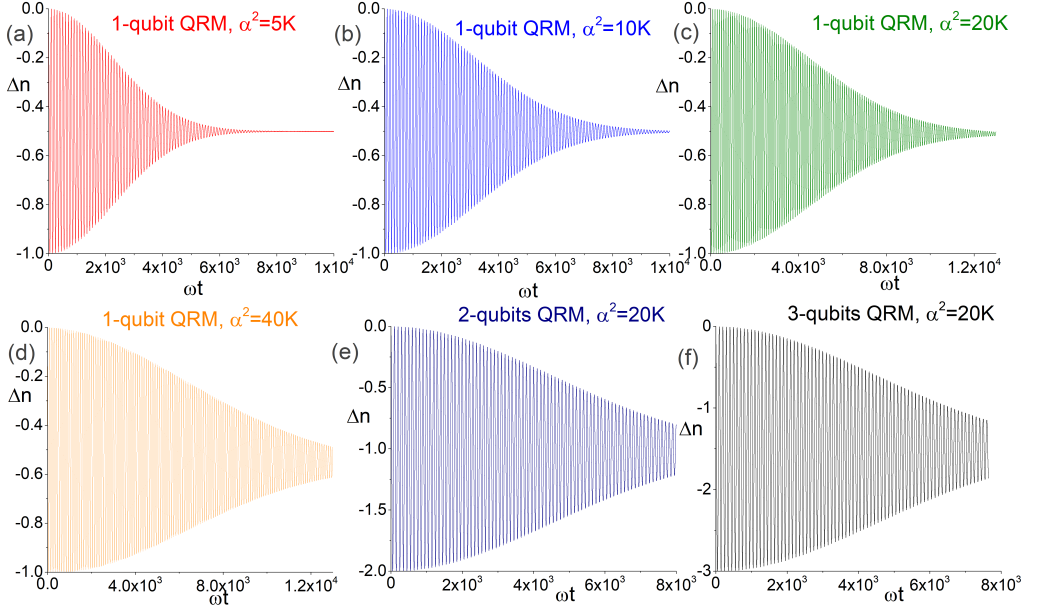


Figure 4.4: Time behavior of the variation of the cavity field average photon number in the lossless QRM. a-d) 1-qubit QRM with $\alpha^2 = 5K$, $10K$, $20K$ and $30K$. e-f) QRM with two and three identical noninteracting qubits, respectively, and $\alpha^2 = 20K$. Notice that in all the cases Δn exhibits a collapse behavior.

collapse process on the same timescale as the qubit. In the panels 4.4e and 4.4f we consider the scenario with two and three noninteracting qubits (with identical parameters) that interact with the cavity field in the initial coherent state with $\alpha^2 = 20K$. We verified that, in this case, the dynamics of each qubit is almost indistinguishable from the dynamics in the 1-qubit setup (shown in Fig. 4.2c). The cavity field exchanges two and three photons with the atoms, respectively, while also undergoing a collapse process.

It is obvious that the qubit(s) become entangled with the cavity field during the evolution, but without numeric calculations it is impossible to infer the amount of entanglement and its dynamical behaviour. To characterize the entanglement of a *pure bipartite system* it is enough to study the von Neumann or the linear entropies of any subsystem, $S_i \equiv -\text{Tr}(\hat{\rho}_i \ln \hat{\rho}_i)$ and $S_i^{(L)} \equiv 1 - \text{Tr}(\hat{\rho}_i^2)$, respectively, where $\hat{\rho}_i$ is the reduced density operator of any subsystem (this is a straightforward consequence of the Schmidt decomposition [29, 34]). For a multipartite system, on the other hand, these entropies only measure the entanglement between the subsystem i and the rest of the system. We chose to study the von Neumann entropy for the qubit, S_q , and the linear entropy for the cavity field, $S_f^{(L)}$. Notice that for the single-qubit QRM we have $S_q^{(L)} = S_f^{(L)}$, so in this case $S_f^{(L)}$ also quantifies the purity of the atom, which is an important figure of merit in Quantum Information protocols. In the panels 4.5a and 4.5b, the solid lines show S_q and $S_f^{(L)}$ as a function of time for QRM (in the case of 2- and 3-qubits QRM, these are the entropies of any qubit and the field, respectively), while the dashed lines show the von Neumann and

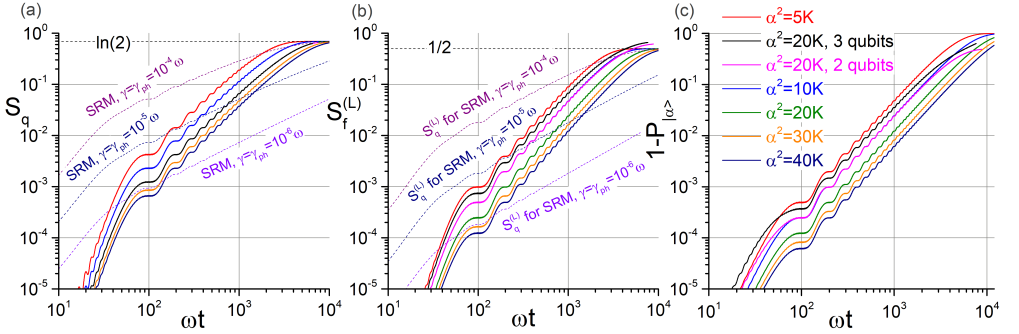


Figure 4.5: a) Dynamics of the von Neumann entropy of a single qubit in the dissipative SRM (dashed lines, assuming $n_{th} = 0.05$) and lossless QRM (solid lines). The parameters and the values of α^2 are indicated in the figure. b) Linear entropy of the cavity field state. c) Probability that the cavity field state does not remain in the original coherent state $|\alpha(t)\rangle$, where $\alpha(t) = \alpha e^{-i\omega t}$. Note: some curves are incomplete, because the simulations were still running at the moment of the writing of this chapter.

the linear entropies of the qubit in the dissipative SRM. We see that the qubit's purity loss due to the exchange of photons with the quantized cavity field is as important as the dissipative effects in SRM when $\gamma, \gamma_{ph} \lesssim 10^{-6}\omega$ (as expected, for larger α the loss of purity is smaller at a given time). We also see that the atom(s) and the field become entangled from the very beginning, and do not disentangle even after a complete Rabi oscillation, attaining a high degree of entanglement for the times of the order of T_{col} (with the maximum allowed values of the entropies, $S_{q,\text{max}} = \ln 2$ and $S_{f,\text{max}}^{(L)} = 1/2$, in the case of a single qubit). Finally, these plots also show that the purity of the atom, due to the quantized nature of the field, differs from 1 by roughly 10^{-4} at the moment of the first complete Rabi oscillation (for the chosen parameters).

We already noticed that the average photon number decreases during the atom-field interaction, so an interesting question is what is the probability of the cavity field remaining in the coherent state $|\alpha(t)\rangle$, where $\alpha(t) = \alpha e^{-i\omega t}$ is the field amplitude (in the interaction picture we are adopting here) that would hold in the absence of the atom(s). To answer this question, we calculated numerically the probability $P_{|\alpha\rangle} = \text{Tr} [\hat{\rho} |\alpha e^{-i\omega t}\rangle \langle \alpha e^{-i\omega t}|]$ of the field remaining in the state $|\alpha(t)\rangle$, and plotted the quantity $1 - P_{|\alpha\rangle}$ in the panel 4.5c. This panel shows that the cavity field state is drastically altered during the evolution and does not return to the freely evolving state $|\alpha(t)\rangle$ for the considered time intervals, as opposed to the SRM assumption that the field remains in the same state throughout the evolution.

To understand why $P_{|\alpha\rangle} \rightarrow 0$ for large times, we studied the photon number distribution for different times. In Fig. 4.6 we show the results for $\alpha^2 = 5\text{K}$. Panel 4.6a shows $\Delta p_n = p_n(t) - p_n(0)$, which is the difference between the photon number distribution at the time t , $p_n(t) = \text{Tr} (\hat{\rho}(t)|n\rangle \langle n|)$, and the initial photon number distribution (shown in the inset), where t is some odd multiple of T_π (corresponding to the local maxima of the atomic excitation probability). The panel 4.6b shows Δp_n for some even multiples of T_π ,

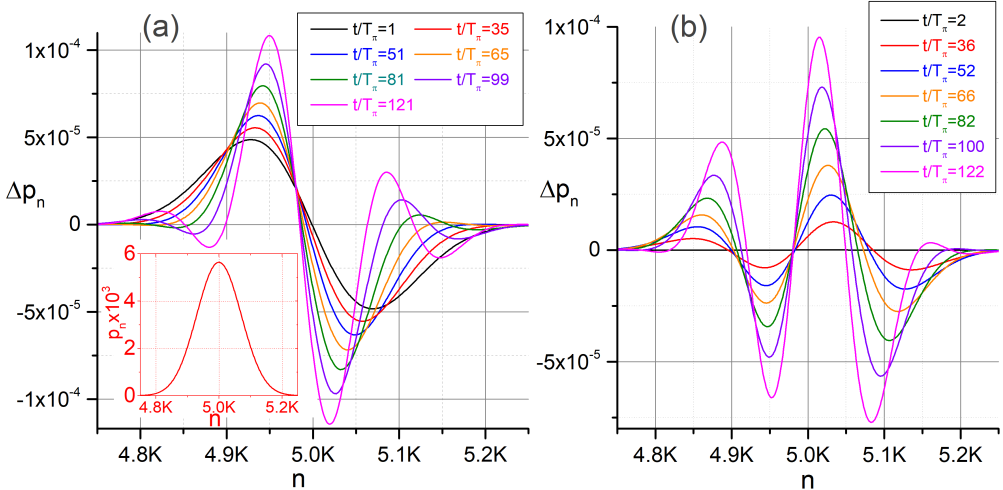


Figure 4.6: a) Modification of the photon number distribution of the cavity state (compared to the initial one) for $\alpha^2 = 5\text{K}$ and odd multiples of T_π , when the qubit excitation probability attains local maxima. The inset shows the original photon number distribution. b) Modification of the photon number statistics at even multiples of T_π , when the atomic excitation probability attains local minima.

when the atomic excitation probability attains a local minimum. In Figures 4.7 and 4.8 we do a similar analysis for $\alpha^2 = 20\text{K}$ (considering the 2- and 3-qubit QRM, as well) and $\alpha^2 = 40\text{K}$, respectively.

We see that for initial times, $t \lesssim 10T_\pi$, the behaviour of Δp_n is intuitive. At the moments of a maximum of P_e (odd multiples of T_π), Δp_n is positive for $n < \alpha^2$ and negative for $n > \alpha^2$; for even multiples of T_π , when the qubit attains the minimum excitation probability, Δp_n is nearly zero. However, for larger times the behaviour becomes more complex, and for even multiples of T_π the field state does not return to its initial statistics. This is consistent with the emergence of the collapse behaviour of P_e and Δn for large times, since the field state does not return to its original state after a complete Rabi oscillation. We also note that, for a given time t , $\Delta p_n(t)$ becomes smaller when α increases (recalling that we assume that $g\alpha$ is constant), so for $\alpha \rightarrow \infty$ and initial times ($t \ll T_{\text{col}}$) the tiny modifications of Δp_n become undetectable experimentally and the semiclassical assumption that the cavity field is not altered during the evolution becomes justified. However, our analysis shows that as the time increases, the semiclassical approximation progressively loses its validity due to a significant modification of the photon number statistics and the entanglement between the cavity field and the atom(s).

4.4.3 Dissipation in the quantum regime

Before concluding this work, let us study numerically how the dissipation affects the system dynamics in the quantum regime, when the total density operator obeys the

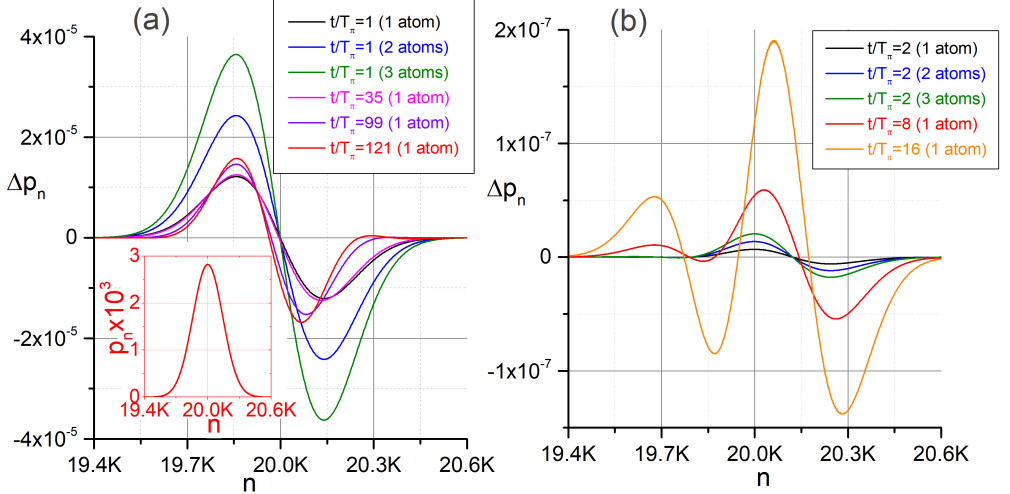


Figure 4.7: Similar to Fig. 4.6 but for $\alpha^2 = 20K$ and contemplating the scenarios with 1, 2 and 3 identical noninteracting qubits coupled to the cavity field.

Lindblad master equation

$$\begin{aligned} \frac{\partial \hat{\rho}}{\partial t} = & -i \left[\hat{H}_{QRM}/\hbar, \hat{\rho} \right] + \frac{\gamma}{2} (n_{th} + 1) \mathcal{D}[\hat{\sigma}_-] \hat{\rho} + \frac{\gamma}{2} n_{th} \mathcal{D}[\hat{\sigma}_+] \hat{\rho} + \frac{\gamma_\phi}{2} \mathcal{D}[\hat{\sigma}_z] \hat{\rho} \\ & + \frac{\kappa}{2} (n_c + 1) \mathcal{D}[\hat{a}] \hat{\rho} + \frac{\kappa}{2} n_c \mathcal{D}[\hat{a}^\dagger] \hat{\rho}, \end{aligned} \quad (4.37)$$

where κ is the cavity damping rate and $n_c = [e^{\hbar\omega/k_B T} - 1]^{-1}$ is the average thermal photon number for the cavity frequency ω and the temperature T . Since for the density matrix the number of elements grows quadratically with the number of photons, we managed to solve numerically the master equation (4.37) only for a relatively weak initial coherent state $|g, a\rangle$ with $\alpha^2 = 50$ (maintaining the previous parameters $\Delta = 0$ and $g\alpha/\omega = 10^{-2}\pi$). In Fig. 4.9 we show the results for the dissipationless case (dark yellow lines) and two different sets of the dissipative parameters: $\gamma = \gamma_\phi = 10^{-5}\omega$, $\kappa = 10^{-6}\omega$ (red lines) and $\gamma = \gamma_\phi = 10^{-4}\omega$, $\kappa = 10^{-5}\omega$ (blue lines), where we assumed $n_{th} = n_c = 0.05$. As expected, in the unitary case there are revivals of P_e and Δn for the integer multiples of $(\omega T_{rev}) \sim 200\alpha^2 = 10^4$. Besides, we see that the linear entropies $S_q^{(L)}$ and $S_f^{(L)}$ do not saturate at some constant values as one could misinterpret from Fig. 4.5; instead, they exhibit oscillatory behaviours on the timescales of the order of T_{rev} , going nearly to zero halfway between the revivals. Such behaviours were not captured by Fig. 4.5 because the necessary time intervals would be $\omega t \gtrsim 100\alpha^2$, and for such long times the effects of dissipation would be dominant. Typical behaviours of the QRM in the presence of dissipation are illustrated by the red and blue solid lines in Fig. 4.9; for the considered dissipative parameters, the dynamics loses the resemblance with the unitary case for times $\omega t \gtrsim 10^4$, and we expect a similar conclusion to hold also for larger values of α (provided $g\alpha$ is maintained constant). Our numeric solution of the master equation shows that, in the presence of dissipation, the revivals of P_e and Δn , as well as

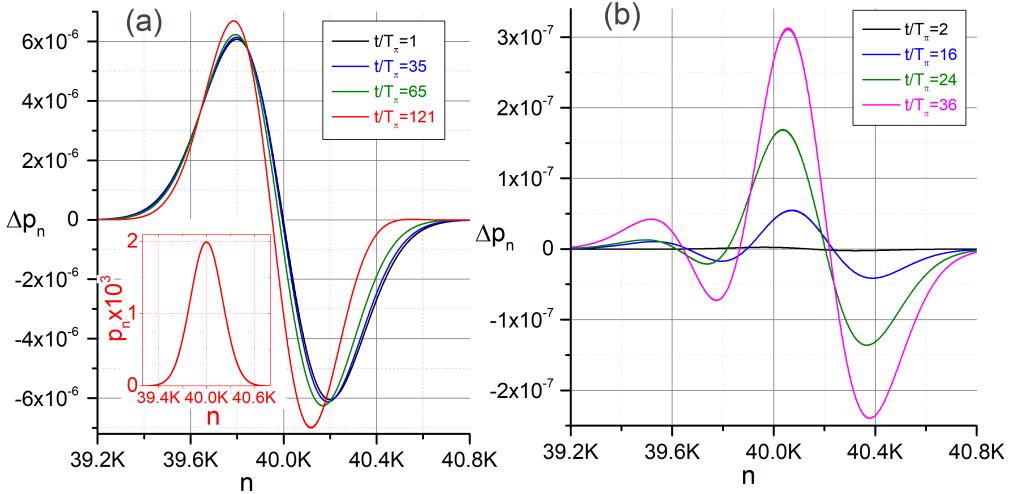


Figure 4.8: Similar to Fig. 4.6 but for $\alpha^2 = 40K$.

the oscillatory behavior of the linear entropies, are first attenuated and then completely eliminated for large times.

Fig. 4.9 also shows that, for the assumed dissipative parameters, the collapse of P_e in the QRM occurs much faster than the semiclassical collapse in the SRM due to the dissipation. The envelope of P_e and the linear entropy $S_q^{(L)}$ (obtained by solving numerically the dissipative SRM with the same parameters as the dissipative QRM) are depicted by the dashed lines in the panels 4.9a and 4.9c, respectively. We see that even in the dissipative case the SRM utterly fails in describing the qubit behaviour when it interacts with a relatively weak coherent state, but for such small values of $\alpha^2 \sim 50$ the failure of SRM was completely expected.

4.5 Summary

In this work we revisited the semiclassical and quantum Rabi models at the exact atom-field resonance. We illustrated how the textbook sinusoidal formula for the Rabi oscillations loses its validity as the duration of the π -pulse decreases below $T_\pi \sim 100\omega^{-1}$ and presented simple analytic and semi-analytic expressions that describe more accurately the behaviour of the atomic excitation probability. Moreover, we carried out detailed numeric simulations of the quantum Rabi model for the initial coherent state with a large average photon number, ranging from 5.000 to 40.000, showing that for initial times the quantum dynamics approaches the semiclassical one (in what concerns the atomic Rabi oscillations), while for larger times the atomic excitation probability inevitably exhibits a collapse behaviour (which is, of course, absent in the semiclassical model). The behaviour of such collapses is qualitatively different from the oscillatory decay of the atomic excited state due to the Markovian damping and dephasing.

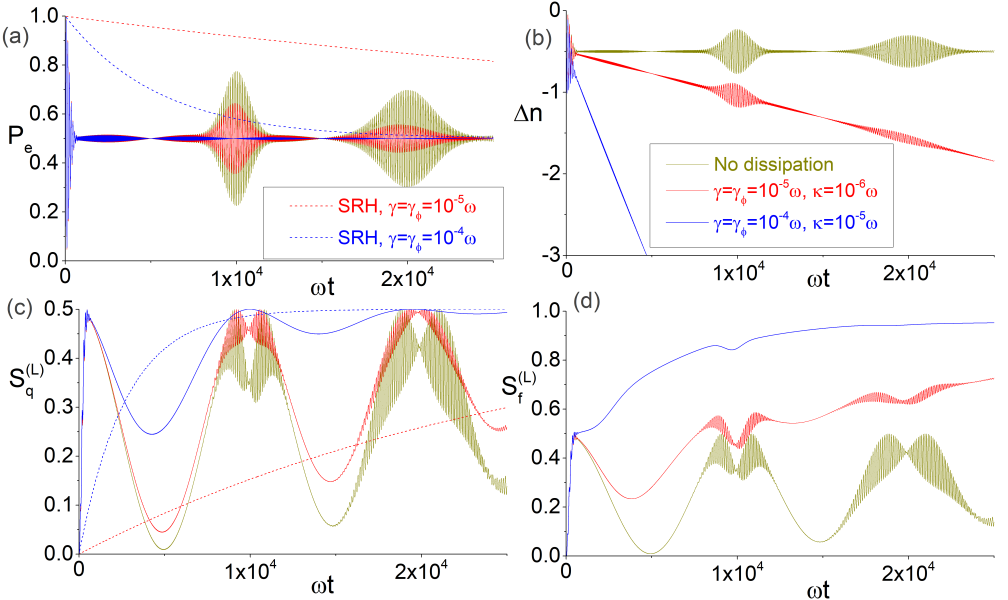


Figure 4.9: Dissipative quantum and semiclassical Rabi models. Solid lines illustrate the time evolution of P_e (panel a), Δn (panel b), $S_q^{(L)}$ (panel c) and $S_f^{(L)}$ (panel d) according to the QRM for different dissipative parameters in the master equation (4.37), assuming $\alpha^2 = 50$, $\omega T_\pi = 50$ and $n_c = n_{th} = 0.05$. The dashed lines illustrate the dissipative behaviour of the envelope of P_e (panel a) and $S_q^{(L)}$ (panel c) according to the SRM.

We believe that the main contribution of this work to the vast literature on the quantum and semiclassical Rabi models was to study numerically the backreaction of the atom on the state of the cavity field, as well as quantifying the atom–field entanglement in the context of the QRM. We showed that the excitation of one or more noninteracting qubits coupled to a single field mode is accompanied by the extraction of a single photon, per atom, from the cavity field; it was also shown that such exchange of excitations ceases for large times due to the collapses of P_e and Δn . Over the course of time the atom becomes entangled with the field, and the system evolves to a maximally entangled state upon the collapse of P_e and Δn (as attested by the maximum values of von Neumann and linear entropies, studied in Figure 4.5); however, from our simulations carried for small values of α , we expect that for large times (of the order of the revival times), the atom–field entanglement should exhibit an oscillatory behaviour. Finally, we studied how the photon number statistics is modified during the evolution, showing that after a complete Rabi oscillation the cavity field does not return to its original state, and for times of the order of the collapse time the probability of finding the field in the original (freely evolving) coherent state tends to zero (although it could exhibit eventual revivals for very long times).

Acknowledgment

A. P. C. acknowledges the financial support by the Brazilian agency Coordenação de Aperfeiçoamento de Pessoal de Nível Superior (CAPES, Finance Code 001). A. D. acknowledges partial financial support of the Brazilian agencies CNPq (Conselho Nacional de Desenvolvimento Científico e Tecnológico) and Fundação de Apoio à Pesquisa do Distrito Federal (FAPDF, grant number 00193-00001817/2023-43).

4.6 References

- [1] M. Le Bellac, *A Short Introduction to Quantum Information and Quantum Computation* (Cambridge University Press, Cambridge, 2012).
- [2] Y. Schön, J. N. Voss, M. Wildermuth, et al. Rabi oscillations in a superconducting nanowire circuit. *npj Quantum Mater.* **5**, 18 (2020).
- [3] Y. Huang, M. T. Amawi, F. Poggiali, F. Shi, J. Du and F. Reinhard, Calibrating single-qubit gates by a two-dimensional Rabi oscillation. *AIP Advances* **13**, 035226 (2023).
- [4] I. I. Rabi. On the Process of Space Quantization. *Phys. Rev.* **49**, 324 (1936).
- [5] I. I. Rabi. Space quantization in a gyrating magnetic field. *Phys. Rev.* **51**, 652 (1937).
- [6] R. Merlin. Rabi oscillations, Floquet states, Fermi's golden rule, and all that: Insights from an exactly solvable two-level model. *Am. J. Phys.* **89**, 26 (2021).
- [7] R. W. Boyd. *Nonlinear Optics* (Academic Press, London, 2nd Edition, 2003).
- [8] M. O. Scully and M. S. Zubairy. *Quantum Optics* (Cambridge University Press, Cambridge, 1997).
- [9] B. W. Shore. Coherent manipulation of atoms using laser light. *Acta Physica Slovaca* **58**, 243 (2008).
- [10] R. Graham and M. Höhnerbach. Two-state system coupled to a boson mode: Quantum dynamics and classical approximations. *Z. Physik B - Cond. Matt.* **57**, 233 (1984).
- [11] M. Munz and G. Marowsky. Rabi-oscillations without rotating-wave approximation. *Z. Phys. B - Condensed Matter* **63**, 131 (1986).
- [12] J. Liu and Z.-Y. Li. Interaction of a two-level atom with single-mode optical field beyond the rotating wave approximation. *Opt. Expr.* **22**, 28671 (2014).
- [13] L.-Z. Lu, D.-Q. Wen, S.-J. Jiang and X.-Y. Yu. Interaction between the ultrashort pulse and two-level medium beyond the rotating wave approximation. *Eur. Phys. J. D* **70**, 184 (2016).
- [14] S. Ashhab. Landau-Zener-Stueckelberg interferometry with driving fields in the quantum regime. *J. Phys. A: Math. Theor.* **50**, 134002 (2017).
- [15] L. O. Castaños. Simple, analytic solutions of the semiclassical Rabi model. *Opt. Commun.* 430, 176 (2019).
- [16] I. Sainz, A. García and A. B. Klimov. Effective and efficient resonant transitions in periodically modulated quantum systems. *Quantum Reports* **3**, 1 (2021).
- [17] I. Sainz, A. B. Klimov and C. Saavedra. Effective Hamiltonian approach to periodically perturbed quantum optical systems. *Phys. Lett. A* **351**, 26 (2006).
- [18] A. Marinho and A. Dodonov. Analytic approach for dissipative semiclassical Rabi model under parametric modulation, in A. Dodonov and C. C. H. Ribeiro (Eds.),

Proceedings of the Second International Workshop on Quantum Nonstationary Systems, pp. 195–210 (LF Editorial, São Paulo, 2024). ISBN: 978-65-5563-446-4.

- [19] A. Marinho and A. V. Dodonov. Approximate analytic solution of the dissipative semiclassical Rabi model under parametric multi-tone modulations. *Phys. Scr.* **99**, 125117 (2024).
- [20] Q. Xie, H. Zhong, M. T Batchelor and C. Lee, The quantum Rabi model: solution and dynamics. *J. Phys. A.: Math. Theor.* **50**, 113001 (2017).
- [21] D. Braak, Q.-H. Chen, M. T. Batchelor and E. Solano. Semi-classical and quantum Rabi models: in celebration of 80 years. *J. Phys. A: Math. and Theor.* **49**, 300301 (2016).
- [22] D. Braak. Integrability of the Rabi model. *Phys. Rev. Lett.* **107**, 100401 (2011).
- [23] J. Larson and Th. K. Mavrogordatos. *The Jaynes-Cummings Model and Its Descendants* (IOP Publishing, Bristol, 2021). <https://arxiv.org/abs/2202.00330> (2024).
- [24] E. K. Irish and A. D. Armour. Defining the semiclassical limit of the quantum Rabi Hamiltonian. *Phys. Rev. Lett.* **129**, 183603 (2022).
- [25] H. F. A. Coleman and E. K. Twyeffort. Spectral and dynamical validity of the rotating-wave approximation in the quantum and semiclassical Rabi models. *J. Opt. Soc. Am. B* **41**, C188 (2024).
- [26] A. Marinho, M. V. S. de Paula and A. V. Dodonov. Approximate analytic solution of the dissipative semiclassical Rabi model near the three-photon resonance and comparison with the quantum behaviour. *Phys. Lett. A* **513**, 129608 (2024).
- [27] H. Carmichael. *An Open System Approach to Quantum Optics* (Springer, Berlin, 1993).
- [28] W. Vogel and D.-G. Welsch. *Quantum Optics* (Wiley, Berlin, 2006).
- [29] M. Orszag. *Quantum Optics* (Springer, Berlin, 2nd Edition, 2008).
- [30] A. V. Dodonov. Errors in zero-excitation state preparation due to anti-rotating terms in two-atom Markovian cavity QED. *Phys. Scr.* **82**, 055401 (2010).
- [31] A. V. Dodonov. Mean excitation numbers due to the anti-rotating term in cavity QED under Lindbladian dephasing. *Phys. Scr.* **86**, 025405 (2012).
- [32] I. M. de Sousa and A. V. Dodonov. Microscopic toy model for the cavity dynamical Casimir effect. *J. Phys. A: Math. Theor.* **48**, 245302 (2015).
- [33] J. H. Eberly, N. B. Narozhny and J. J. Sanchez-Mondragon. Periodic spontaneous collapse and revival in a simple quantum model. *Phys. Rev. Lett.* **44**, 1323 (1980).
- [34] M. A. Nielsen and I. L. Chuang. *Quantum Computation and Quantum Information* (Cambridge University Press, Cambridge, 10th Edition, 2010).